

Finite-temperature properties of the extended Heisenberg model on a triangular lattice

P. Prelovšek^{1,2} and J. Kokalj^{3,1}

¹*Jožef Stefan Institute, SI-1000 Ljubljana, Slovenia*

²*Faculty of Mathematics and Physics, University of Ljubljana, SI-1000 Ljubljana, Slovenia*

³*Faculty of Civil and Geodetic Engineering, University of Ljubljana, SI-1000 Ljubljana, Slovenia*

We present numerical results for the J_1 - J_2 Heisenberg model on a triangular lattice at finite temperatures $T > 0$. In contrast to unfrustrated lattices we reach much lower $T \sim 0.15J_1$. In static quantities the novel feature is a quite sharp low- T maximum in the specific heat. Dynamical spin structure factor $S(\mathbf{q}, \omega)$ allows for the extraction of the effective spin-wave energies $\omega_{\mathbf{q}}(T)$ and their damping $\gamma_{\mathbf{q}}(T)$. While for $J_2 = 0$ our results are consistent with $T = 0$ spin ordering, $J_2/J_1 \sim 0.1$ induces additional frustration with a signature of spin liquid ground state. In the latter case, results for spin-lattice relaxation rate indicate in the low- T accessible regime on $1/T_1 \propto T^\alpha$ with $\alpha \geq 1$, as observed in recent spin-liquid materials on a triangular lattice.

Introduction. In the last decade there are intensive theoretical efforts to understand spin systems, which would behave at low temperatures T as spin liquids (SL) [1], i.e., revealing no long-range order (LRO) down to $T \rightarrow 0$. The theoretical search [2] has been stimulated by several novel materials, which seem to be realization of frustrated two-dimensional (2D) spin systems and experiments allow for the measurements of various static and dynamical properties [3]. As a very recent candidate with a triangular lattice (TL) is a layered material 1T-TaS₂, which has at $T < T_{CDW}$ a commensurate charge-density-wave (CDW) order, but is a Mott insulator [4] without any spin order at $T \rightarrow 0$ [5–8]. Nevertheless, the nuclear-relaxation measurements reveal spin fluctuations within the charge gap and spin-lattice relaxation $1/T_1 \propto T^\alpha$ with $\alpha \sim 2$ in a broad range $T_f < T < T_{CDW}$. Analogous relaxation is observed in organic compound κ -(ET)₂Cu₂(CN)₃ [3, 9, 10] with $\alpha \sim 1.5$ and EtMe₃Sb[Pd(dmit)₂]₂ with $\alpha \sim 2$ [11]. All these results indicate on relevant low-energy spin fluctuations and support the interpretation in terms of a SL, behaving as gapless at least in a certain T range.

Antiferromagnetic (AFM) Heisenberg model (HM) on TL has been originally proposed [12] as the candidate for the resonant-valence-bond or SL ground state (g.s.). Numerical [13–15] and analytical [16] studies, however, reveal that g.s. has spiral LRO with spins pointing along 120° tilted directions. Recently, the focus shifted to generalized HM where SL can become the stable g.s.. Recent numerical studies reveal that the $J_1 - J_2$ HM on TL with additional AFM next-neighbor coupling $J_2 > 0$ introduces further frustration which favours SL [17–22]. The same state might be stable also by introducing ring-exchange [23, 24] or similar terms obtained by downfolding the Hubbard model in the Mott insulating phase [25, 26]. Much less firm are conclusions on $T > 0$ properties. It is plausible that within a simple HM on TL frustration reduces LRO relative to unfrustrated square lattice [27]. Still, numerical calculations of static quantities

within the HM on TL [28] did not pin down evident $T > 0$ features with a dominant effect of SL physics. In particular, the consequences for local spin correlations $S_L(\omega)$, as measured via NMR spin-lattice relaxation $1/T_1$, remain an open theoretical question in frustrated spin systems [3], but not fully clarified on the square lattice either [27, 29–31].

In this Letter we present $T > 0$ results for the $J_1 - J_2$ HM on TL obtained by the finite- T Lanczos method (FTLM) [32–34]. One feature (not present on a square lattice) appears in the specific heat $C_V(T)$, revealing a broad shoulder at $T < J_1$ ending with a pronounced peak at $T_{coh} \sim 0.15 - 0.25J_1$, least pronounced for the SL candidate at $J_2 \sim 0.1J_1$. One can associate such a behavior with the onset of spin coherence (long- or short-range) only at $T \sim T_{coh} \ll J_1$. At $J_2 = 0$ we observe the softening of the ‘spin-wave’ (SW) energies $\omega_{\mathbf{q}}(T)$ as $T \rightarrow 0$ in the Brillouin zone (BZ) corner, consistent with the g.s. LRO [13–15] and the SW approximation [16]. However, small $J_2/J_1 \sim 0.1$ already induces near degeneracy at the BZ edges, favouring the interpretation in terms of SL. The most elusive conclusion so far has been the dynamical SW damping $\gamma_{\mathbf{q}}(T)$, which we find at lowest reachable T decreasing with T . Consistently, we find in the SL regime at low but reachable T above finite size $T_{fs} \sim 0.15J_1$ the relaxation rate behaving as $1/T_1 \propto T^\alpha$ with $\alpha \geq 1$, qualitatively in agreement with recent results in candidate SL materials [3, 5].

Model and numerical method. We consider the isotropic J_1 - J_2 extended HM on TL,

$$H = J_1 \sum_{\langle ij \rangle} \mathbf{S}_i \cdot \mathbf{S}_j + J_2 \sum_{\langle\langle ij \rangle\rangle} \mathbf{S}_i \cdot \mathbf{S}_j, \quad (1)$$

for local spins $S = 1/2$ with AFM nearest-neighbor spin exchange J_1 and next-nearest neighbor exchange $J_2 \geq 0$. J_2 introduces additional frustration. Further on we set $J_1 = 1$ as an energy scale. We consider the model on 2D lattices with periodic boundary conditions with up to $N = 30$ sites according to minimal imperfection [35–37] and the possibility to contain particular wavevector

\mathbf{Q} within the BZ. Within the triangular lattice of particular interest are BZ corner $\mathbf{Q}_K = (4\pi/3, 0)$ relevant for the 120° spiral LRO, $\mathbf{Q}_M = (0, 2\pi/\sqrt{3})$ dominant in the stripe-like ordering at $J_2 \geq 0.15$ [21] or for square-lattice-like AFM order on anisotropic TL [24].

We calculate thermodynamic quantities and dynamical structure factor $S(\mathbf{q}, \omega)$ at $T > 0$, using the FTLM [32, 33], previously used in numerous studies of $T > 0$ properties in various models of correlated electrons [34]. The main limitation of the method are finite size effects appearing for $T < T_{fs}$. While for HM on a square lattice we reach $T_{fs} \sim 0.4$ [33, 34], the frustration due to TL and $J_2 > 0$ allows to reach considerably lower $T_{fs} \sim 0.15$. See more details in [37] where for example the specific heat $C_V(T)$ showing consistent behavior for a wide range of lattices $N = 20 - 30$ down to $T \sim 0.15$ is presented. We note also that FTLM has been recently used also to evaluate $T > 0$ properties of HM and Hubbard model on an anisotropic TL [38, 39].

Thermodynamic quantities. The difference between the HM on a square lattice and on TL is well visible already in the entropy density $s(T)$ (in units of k_B) and in the related specific heat $C_V(T)$. Corresponding results for $J_2 = 0, 0.1, 0.2$, along with results for the square lattice, as obtained by FTLM on $N = 30$ lattice, are presented in Fig. 1. While in both models the entropy $s(T)$ saturates at $T > 1$, the behavior evidently splits at $T < 1$. On square lattice the onset of short-range order at $T < 1$ can be associated with a drop of $s(T)$, coinciding with the maximum in C_V at $T = T_{coh} \sim 0.7$. On the other hand, large $s(T)$ persists on TL to lower T and the inflection point shifts to $T_{coh} \sim 0.2$ for $J_2 = 0$ and even lower for $J_2 = 0.1, 0.2$. The behavior is reflected in $C_V(T)$ on TL, which reveals (in contrast to square lattice) a broad shoulder at $T < 1$, but as well a peak appearing at lower $T_{coh} = 0.15 - 0.25$. The latter is most pronounced and stable [37] at $J_2 = 0$, consistent with the onset of LRO in this case and in agreement with increased static correlations $S_{\mathbf{q}}$ and susceptibilities $\chi_{\mathbf{q}}^0$ for $T < T_{coh}$ [37]. It has been apparently missed in some previous studies [28], but observed within Hubbard model on the anisotropic TL [39]). The peak in $C_V(T)$ is weakest for $J_2 \sim 0.1$, another signature for low- T SL, while it reappears for $J_2 = 0.2$ with the presumable onset of the stripe order. In contrast to $C_V(T)$ the uniform susceptibility $\chi_0(T)$ is more featureless [37].

Dynamical spin structure factor. Next we turn to the dynamical spin structure factor $S(\mathbf{q}, \omega)$, evaluated within FTLM [33, 34] with similar restrictions as the thermodynamic quantities above. Due to periodic boundary conditions we are restricted to discrete \mathbf{q} within the BZ (see the inset in Fig. 2 for the $N = 30$ lattice). It is helpful to analyse $S(\mathbf{q}, \omega)$ in terms of the dynamical susceptibilities $\text{Im}\chi_{\mathbf{q}}(\omega) = \pi(1 - e^{-\beta\omega})S(\mathbf{q}, \omega)$ whereby (complex) $\chi_{\mathbf{q}}(\omega)$ can be represented in the form of the memory function

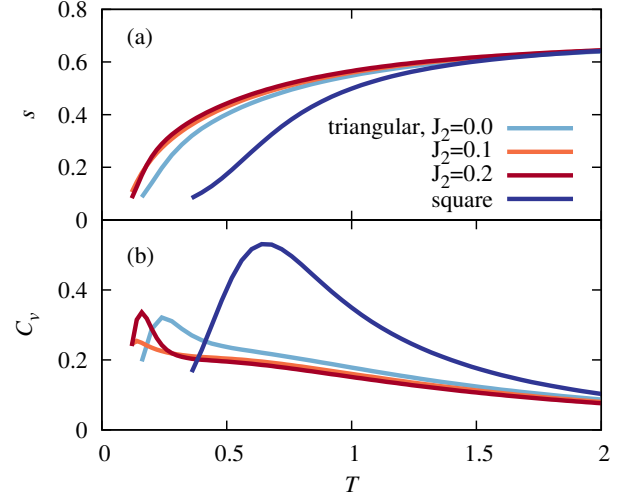


Figure 1. (a) The entropy density $s(T)$, and b) specific heat $C_V(T)$ of the J_1 - J_2 Heisenberg model on the triangular lattice for different J_2 , and compared to the reference square-lattice result, as obtained by FTLM on lattices with $N = 30$ sites.

(MF) $M_{\mathbf{q}}(\omega)$ [40–42] (for relations see [37]),

$$\chi_{\mathbf{q}}(\omega) = \frac{-\eta_{\mathbf{q}}}{\omega^2 - \omega_{\mathbf{q}}^2 + \omega M_{\mathbf{q}}(\omega)}, \quad (2)$$

with the effective SW energy $\omega_{\mathbf{q}}^2 = \eta_{\mathbf{q}}/\chi_{\mathbf{q}}^0$, $\chi_{\mathbf{q}}^0 = \chi_{\mathbf{q}}(\omega = 0)$ and $\eta_{\mathbf{q}}$ the corresponding stiffness. Both $\chi_{\mathbf{q}}^0$ and $\eta_{\mathbf{q}}$ can be directly evaluated from numerically calculated $S(\mathbf{q}, \omega)$, while the latter allows also to extract $M_{\mathbf{q}}(\omega)$ [37]. We note that $\gamma_{\mathbf{q}}(\omega) = \text{Im}M_{\mathbf{q}}(\omega)$ has a direct interpretation in terms of the damping of the SW mode at $\omega_{\mathbf{q}}$. The analysis in terms of Eq. (2) is general, but it becomes particularly meaningful provided that $\gamma_{\mathbf{q}}(\omega)$ is weakly ω and \mathbf{q} dependent, especially for \mathbf{q} along the BZ boundary, where $\omega_{\mathbf{q}}$ are smallest (and $\chi_{\mathbf{q}}^0$ largest). We note that $\eta_{\mathbf{q}}$ (expressed in terms of local static correlations [37]) is (away from $q = 0$) generally modestly \mathbf{q} and T dependent.

Results for $\chi_{\mathbf{q}}^0$, presented in Fig. 2a, reveal crucial dependence on J_2 . We compare $\chi_{\mathbf{q}}^0(T)$ on TL for three parameters $J_2 = 0, 0.1, 0.2$ and for three characteristic \mathbf{q} : BZ corner \mathbf{Q}_K and edge \mathbf{Q}_M , and for reference also the inside-BZ point \mathbf{Q}_X (where SW approximation at $J_2 = 0$ yields the maximum $\omega_{\mathbf{q}} \sim 1.5$ [16]), which are accessible on $N = 30$ lattice (see inset in Fig. 2). Several conclusions can be drawn from Fig. 2a: a) $\chi_{\mathbf{q}}^0(T)$ have strong T dependence and much larger values for \mathbf{q} along the BZ boundaries relative to inside of BZ (as well to $\chi_0(T)$ [37]). b) The variation with J_2 shows the qualitative change of spin excitations. For $J_2 = 0$ the value at \mathbf{Q}_K is clearly dominant over \mathbf{Q}_M , consistent with divergence of $\chi_K^0(T \rightarrow 0)$ and the spiral g.s. LRO. This is not the case for $J_2 = 0.1$ where $\chi_M^0(T) \sim \chi_K^0(T)$ with an increase for lower $T \sim T_{fs}$, whereby we cannot give a firm conclu-

sion on the behavior of $\chi_{\mathbf{q}}^0(T \rightarrow 0)$. Finally, for $J_2 = 0.2$ the situation is inverted relative to $J_2 = 0$, with dominant and apparently diverging $\chi_M^0(T \rightarrow 0)$, indicating a stripe g.s. LRO. c) Presented results for $\chi_{\mathbf{q}}(T \rightarrow 0)$ are qualitatively consistent with previous numerical studies of the g.s. of the J_1 - J_2 HM on TL, dealing with static (equal-time) correlations $S_{\mathbf{q}} = (1/\pi) \int d\omega S(\mathbf{q}, \omega)$ [17, 19, 21, 22] which also show a qualitative change along the J_2 phase diagram (for our $S_{\mathbf{q}}(T)$ results see [37]). In contrast to $S_{\mathbf{q}}(T)$ the susceptibility $\chi_{\mathbf{q}}^0(T)$ incorporates also information on dynamical softening, and enhances differences between low- T regimes.

Corresponding $\omega_{\mathbf{q}}(T)$ are presented in Fig. 2b and mainly reflect the behavior of $\chi_{\mathbf{q}}^0(T)$. Results are qualitatively consistent with the softening of SW mode $\omega_K(T \rightarrow 0) = 0$ at $J_2 = 0$, and similarly $\omega_M(T \rightarrow 0) = 0$ for $J_2 = 0.2$, respectively. On contrary, consistent with the SL scenario $\omega_{\mathbf{q}}(T \rightarrow 0)$ only partially softens in the intermediate case $J_2 = 0.1$ with near degeneracy of $\omega_K \sim \omega_M$ down to lowest T . Results for $\omega_{\mathbf{q}}(T)$ could be qualitatively interpreted in terms SW-approximation result $\tilde{\omega}_{\mathbf{q}}$ [16] generalized via an effective gap $\kappa(T)$ (at least along the BZ boundary) into $\omega_{\mathbf{q}}^2 \sim \tilde{\omega}_{\mathbf{q}}^2 + \kappa^2$, which can as well be associated with the finite AFM correlation length $\xi \sim v_0/\kappa$, where $v_0 \sim 1$ is the AFM magnon velocity [16] (at $J_2 = 0$). In such a scenario, results confirm that in HM on TL the longer correlation length, i.e., $\kappa(T) < 1$ emerges only at $T < 0.5$, below which $\omega_{\mathbf{q}}$ start to differentiate. I.e., for $J_2 = 0$ $\omega_K(T)$ is decreasing with $T \rightarrow 0$, while ω_X increases towards the SW-approximation result $\omega_X \sim 1.6$ [16]. The role of K and M are reversed for $J_2 = 0.2$, while most interesting $J_2 = 0.1$ reveals besides the degeneracy $\omega_K \sim \omega_M$ and $\kappa(T) > 0.7$ also weak T dependence, at least for reachable $T \sim T_{fs}$.

Although one might suspect that damping $\gamma_{\mathbf{q}}(\omega)$ is more sensitive quantity (which is anyhow the case due to numerical and finite-size limitations), results confirm that it is (some characteristic cases shown in [37]) quite ω independent, at least within the relevant range $\omega \lesssim \omega_{\mathbf{q}}$. This reduces Eq. (2) to a form of simple damped oscillator [37]. In Fig. 3 we show results for the d.c. limit $\gamma_{\mathbf{q}}^0 = \gamma_{\mathbf{q}}(\omega \rightarrow 0)$ which reveal that it is moreover weakly \mathbf{q} dependent. At high $T > 0.5$ we get $\gamma_{\mathbf{q}}^0 \sim 2$, in comparison to $\omega_{\mathbf{q}} \gtrsim 1$ in Fig. 2b confirming well damped excitations within the whole BZ. For $T < 0.5$ $\gamma_{\mathbf{q}}^0$ decreases more strongly than $\omega_{\mathbf{q}}$ and leads to more underdamped excitations in particular for \mathbf{Q}_K at $J_2 = 0$ and \mathbf{Q}_M at $J_2 = 0.2$.

NMR spin-lattice relaxation. For the interpretation of NMR spin-lattice relaxation time T_1 the important relation is with low ω dynamical local spin correlations $S_L(\omega) = (1/N) \sum_{\mathbf{q}} S(\mathbf{q}, \omega)$. Assuming \mathbf{q} -independent form factor it follows from Eq. (2),

$$\frac{1}{T_1} \propto S_L(\omega \rightarrow 0) = \frac{T}{\pi N} \sum_{\mathbf{q}} \frac{\eta_{\mathbf{q}} \gamma_{\mathbf{q}}^0}{\omega_{\mathbf{q}}^4}. \quad (3)$$

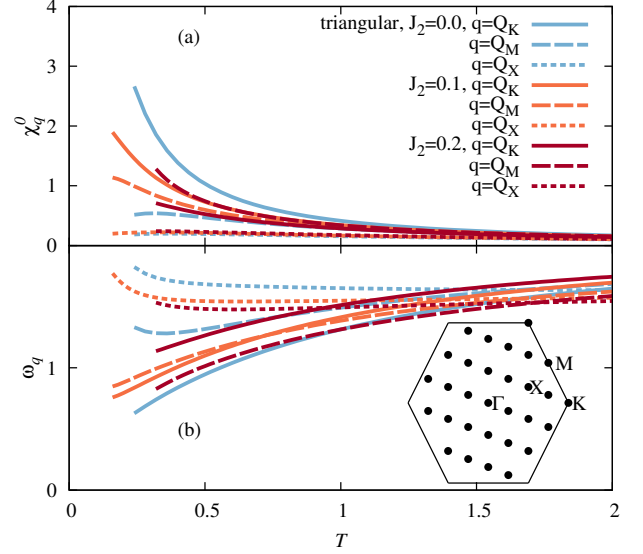


Figure 2. a) Static susceptibilities $\chi_{\mathbf{q}}^0(T)$, and b) corresponding $\omega_{\mathbf{q}}(T)$ on TL for different $J_2 = 0, 0.1, 0.2$, presented for different \mathbf{q} : corner K , edge M and inside X BZ points, respectively. Inset shows the BZ and available \mathbf{q} on $N = 30$ lattice.

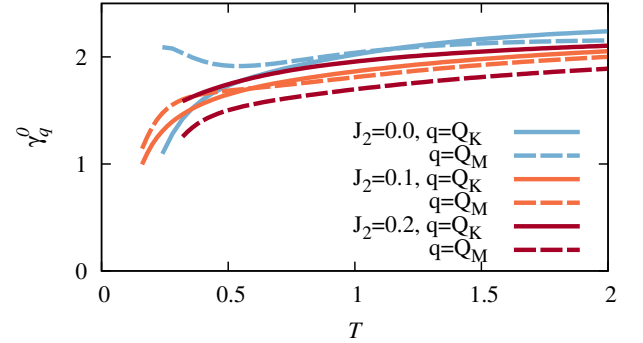


Figure 3. D.c. damping $\gamma_{\mathbf{q}}^0(T)$ for different $J_2 = 0, 0.1, 0.2$ at two BZ-edge wavevectors for $N = 30$ lattice.

Results of a straightforward FTLM calculation of $1/T_1$ obtained on $N = 30$ system (omitting the $q = 0$ contribution) are presented in Fig. 4 for the TL with different J_2 , along with the corresponding result for the square lattice. Using Eq. (3), results can be interpreted as follows. For $T > 1$ $S_L(\omega \sim 0)$ becomes T -independent, so we get $1/T_1 \sim \text{const.}$ [43], with the value quite insensitive to lattice as well as on J_2 . Such behavior extends for TL even further to $T > 0.5$. At lower T the T variation enters through Eq. (3) via $\omega_{\mathbf{q}}(T)$ and $\gamma_{\mathbf{q}}(T)$, where the dominant contribution to $S_L(\omega)$ emerges from soft modes $\omega_{\mathbf{q}} < 1$ inside the BZ. One can simplify the discussion with the observation that the damping is quite \mathbf{q} independent, i.e., $\gamma_{\mathbf{q}}^0 \sim \gamma^0$, while $\eta_{\mathbf{q}} = \eta^0$ is, moreover, T inde-

pendent. From Eq. (3) we then arrive at the estimate for the T -dependence as $1/T_1 \propto T\gamma^0(T)S(T)/\kappa^4(T)$, where $S(T)$ is the BZ surface satisfying $\omega_{\mathbf{q}} \sim \kappa$. Several different scenarios can be now anticipated from the preceding relation for low T :

a) In the case of g.s. LRO in 2D the divergent AFM correlation length is expected as $\kappa = 1/\xi \propto e^{-A/T}$ [44]. Since in 2D $S \propto \kappa^2$ and diverging $\xi(T \rightarrow 0)$ dominates over vanishing $\gamma^0 \propto T^\zeta$, this leads finally to diverging $1/T_1(T \rightarrow 0) \rightarrow \infty$ [29–31]. Due to finite size (restricted number of \mathbf{q}) this behavior is quite hard to establish numerically. Still, we find a reproducible upturn in agreement with such a scenario in Fig. 4, both for the square lattice with an upturn at $T \sim 0.7$, as well in the TR lattice with $J_2 = 0$ with the minimum of $1/T_1$ at $T \sim 0.5$. From our results in Fig. 4 it is not clear whether an analogous scenario should finally (at $T \rightarrow 0$) also apply to stripe order at $J_2 = 0.2$.

b) In a SL regime spin LRO does not emerge at $T \rightarrow 0$. This is reflected either in the saturation $\kappa(T \rightarrow 0) \sim \kappa^0$ or very slowly varying and possibly vanishing $\kappa(T \rightarrow 0) \rightarrow 0$. In the range of our method it is hard to distinguish both options, nevertheless one of them appears to be the case at intermediate $J_2 \sim 0.1$. This still offers several scenarios for the SL. Finite limiting $\gamma^0(T \rightarrow 0)$, with $\kappa_0 > 0$ would indicate on fermionic-type excitations and a gapless SL with spinon Fermi surface [7, 8], leading to $1/T_1 \propto T$, not excluded by results on Figs. 2b and 3. The vanishing $\gamma^0(0)$, which appears more plausible from Fig. 3, at finite $\kappa_0 > 0$ would imply a gapped SL. In this case, observed power-law-like $1/T_1 \propto T^\alpha$ with $\alpha \geq 1$ at $T < T_{coh}$ would crossover into an low- T exponential dependence. On the other hand, slowly vanishing $\kappa(T \rightarrow 0) \rightarrow 0$ would allow also for more involved scenarios, as the gapless Dirac SL, which would lead to $\alpha = 2$ [7], not inconsistent with Fig. 4.

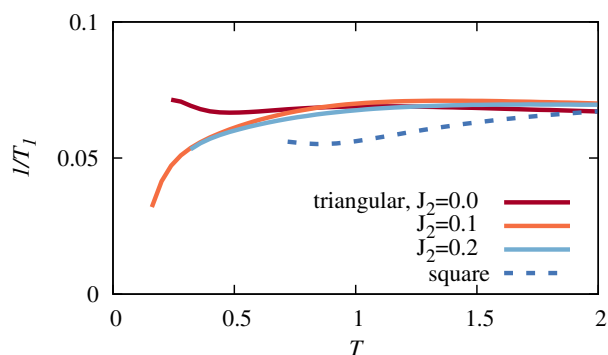


Figure 4. Spin-lattice relaxation rate $1/T_1$ vs. T for the HM on TL with different $J_2 = 0 - 0.2$. For comparison the result for the square lattice is also shown.

Conclusions. Presented results of $T > 0$ static and dynamical properties of 2D J_1 - J_2 HM on TL are com-

plementary to several established and recent studies of the g.s. of the same model. The comparison with better understood HM on square lattice is quite informative. One evident difference is that relative to latter case, the frustration allows for reliable results to much lower, i.e., $T_{fs} \sim 0.15J_1$ for the most frustrated case $J_2 \sim 0.1$. In the specific heat $C_V(T)$ this enables to establish (in contrast to square lattice) two characteristic scales. Besides the broad shoulder at $T < J_1$, we find in TL quite sharp peak at $T \sim (0.15 - 0.2)J_1$ indicating the onset of spin coherence, pronounced in particular for $J_2 = 0$ case.

The focus is still on $T > 0$ dynamical properties, not much accessible so far, in particular those relevant for recent experiments on SL. For the $J_2 = 0$ we find softening of the BZ corner mode $\omega_K(T \rightarrow 0) \rightarrow 0$ [13–15] as well as expected increasing NMR relaxation rate $1/T_1$ by lowering T , as expected for systems with AFM LRO [29, 30]. Most interesting is clearly the intermediate regime $J_2/J_1 \sim 0.1$ as the candidate for SL. Here, down to lowest T a near degeneracy along the BZ edge remains, i.e. $\omega_K \sim \omega_M$ showing tendency of finite limiting $T \rightarrow 0$ value in for low T regime, e.g., for $T_{fs} < T < T_{coh}$. Together with decreasing damping $\gamma_0(T \rightarrow 0)$, this leads to observed vanishing $1/T_1 \propto T^\alpha$ with $\alpha \geq 1$ in the lowest reachable T regime. Such a behavior is an experimental hallmark of a SL, established with $\alpha \sim 2$ in several recent experiments [3, 5]. Still, from our study it is hard to distinguish whether this is intermediate T dependence within a possible gapped SL, or an indication of a gapless SL, e.g., with spinon Fermi-surface with $\alpha = 1$, or a Dirac SL with $\alpha = 2$.

This work is supported by the program P1-0044 of the Slovenian Research Agency.

-
- [1] L. Balents, “Spin liquids in frustrated magnets,” *Nature* **464**, 199–208 (2010).
 - [2] P. A. Lee, “An end to the drought of quantum spin liquids,” *Science* (New York, N.Y.) **321**, 1306–1307 (2008).
 - [3] Y. Zhou, K. Kanoda, and T. K. Ng, “Quantum spin liquid states,” *Rev. Mod. Phys.* **89**, 025003 (2017).
 - [4] E. Tosatti and P. Fazekas, “On the nature of the low-temperature phase of 1T-TaS₂,” *J. Phys.* **37**, 185 (1976).
 - [5] M. Klanjšek, A. Zorko, R. Žitko, J. Mravlje, Z. Jagličić, P. K. Biswas, P. Prelovšek, D. Mihailovic, and D. Arčon, “A high-temperature quantum spin liquid with polaron spins,” *Nature Physics* **13**, 1130–1134 (2017).
 - [6] M. Kratochvilova, A. D. Hillier, A. R. Wildes, L. Wang, S.-W. Cheong, and J.-G. Park, “The low-temperature highly correlated quantum phase in the charge-density-wave 1T-TaS₂ compound,” *Quantum Mat.* **2**, 42 (2017), 1706.04735.
 - [7] K. T. Law and P. A. Lee, “1T-TaS₂ as a quantum spin liquid,” *Proc. Nat. Ac. Sc.* **2017**, 201706769 (2017).
 - [8] W.-Y. He, X. Y. Xu, G. Chen, K. T. Law, and P. A. Lee, “Spinon Fermi surface in a cluster Mott insulator model on a triangular lattice and possible application to

- 1T-TaS₂, url = <http://arxiv.org/abs/1803.00999>, year = 2018,” arXiv:1803.00999.
- [9] Y. Shimizu, K. Miyagawa, K. Kanoda, M. Maesato, and G. Saito, “Spin liquid state in an organic Mott insulator with a triangular lattice,” *Phys. Rev. Lett.* **91**, 107001 (2003), 0307483v1.
 - [10] Y. Shimizu, K. Miyagawa, K. Kanoda, M. Maesato, and G. Saito, “Emergence of inhomogeneous moments from spin liquid in the triangular-lattice Mott insulator ??-(ET) 2 Cu₂ (CN) 3,” *Phys. Rev. B* **73**, 2–5 (2006).
 - [11] T. Itou, A. Oyamada, S. Maegawa, and R. Kato, “Instability of a quantum spin liquid in an organic triangular-lattice antiferromagnet,” *Nature Physics* **6**, 673–676 (2010).
 - [12] P. W. Anderson, “Resonating valence bonds: a new kind of insulator ?” *Mat. Res. Bull.* **8**, 153–160 (1973).
 - [13] B. Bernu, P. Lecheminant, C. Lhuillier, and L. Pierre, “Exact spectra, spin susceptibilities, and order parameter of the quantum heisenberg antiferromagnet on the triangular lattice,” *Phys. Rev. B* **50**, 10048–10062 (1994).
 - [14] L. Capriotti, A. E. Trumper, and S. Sorella, “Long-range néel order in the triangular heisenberg model,” *Phys. Rev. Lett.* **82**, 3899–3902 (1999).
 - [15] S. R. White and A. L. Chernyshev, “Neel order in square and triangular lattice heisenberg models,” *Phys. Rev. Lett.* **99**, 2–5 (2007), 0705.2746.
 - [16] A. L. Chernyshev and M. E. Zhitomirsky, “Spin waves in a triangular lattice antiferromagnet: Decays, spectrum renormalization, and singularities,” *Phys. Rev. B* **79**, 144416 (2009), 0901.4803.
 - [17] R. Kaneko, S. Morita, and M. Imada, “Gapless spin-liquid phase in an extended spin 1/2 triangular Heisenberg model,” *J. Phys. Soc. Japan* **83**, 2–5 (2014), 1407.0318.
 - [18] K. Watanabe, H. Kawamura, H. Nakano, and T. Sakai, “Quantum spin-liquid behavior in the spin-1/2 random heisenberg antiferromagnet on the triangular lattice,” *J. Phys. Soc. Japan* **83**, 1–6 (2014).
 - [19] Z. Zhu and S. R. White, “Spin liquid phase of the S=1/2 J1-J2 Heisenberg model on the triangular lattice,” *Phys. Rev. B* **92**, 041105 (2015).
 - [20] W. J. Hu, S. S. Gong, W. Zhu, and D. N. Sheng, “Competing spin-liquid states in the spin-12 Heisenberg model on the triangular lattice,” *Phys. Rev. B* **92**, 1–6 (2015).
 - [21] Y. Iqbal, W.-J. Hu, R. Thomale, D. Poilblanc, and F. Becca, “Spin liquid nature in the Heisenberg,” *Phys. Rev. B* **93**, 144411 (2016), 1601.06018.
 - [22] S. S. Gong, W. Zhu, J. X. Zhu, D. N. Sheng, and K. Yang, “Global phase diagram and quantum spin liquids in spin-1/2 triangular antiferromagnet,” *CM* , 64–66 (2017).
 - [23] G. Misguich, C. Lhuillier, B. Bernu, and C. Waldtmann, “Spin-liquid phase of the multiple-spin exchange Hamiltonian on the triangular lattice,” *Phys. Rev. B* **60**, 1064–1074 (1999).
 - [24] Michael Holt, Ben J. Powell, and Jaime Merino, “Spin-liquid phase due to competing classical orders in the semi-classical theory of the heisenberg model with ring exchange on an anisotropic triangular lattice,” *Phys. Rev. B* **89**, 174415 (2014).
 - [25] H. Y. Yang, A. M. Lauchli, F. Mila, and K. P. Schmidt, “Effective spin model for the spin-liquid phase of the Hubbard model on the triangular lattice,” *Phys. Rev. Lett.* **105**, 1–4 (2010).
 - [26] K. Misumi, T. Kaneko, and Y. Ohta, “Mott transition and magnetism of the triangular-lattice Hubbard model with next-nearest-neighbor hopping,” , 1–8 (2017), arXiv:1701.08904.
 - [27] E. Manousakis, “The spin-1/2 Heisenberg antiferromagnet on a square lattice and its application to cuprous oxides,” *Rev. Mod. Phys.* **63** (1991).
 - [28] N. Elstner, R. Singh, and a. Young, “Finite temperature properties of the spin-1/2 Heisenberg antiferromagnet on the triangular lattice,” *Phys. Rev. Lett.* **71**, 1629–1632 (1993).
 - [29] S. Tyč, B. I. Halperin, and S. Chakravarty, “Dynamic Properties of a Two-Dimensional Heisenberg Antiferromagnet at Low Temperatures,” *Phys. Rev. Lett.* **62**, 835–838 (1989).
 - [30] Stephane Tyc and B. I. Halperin, “Damping of spin waves in 2D Heisenberg at low T,” *Phys. Rev. B* **42**, 2096–2115 (1990).
 - [31] N. Bulut, W. Hone, D. J. Scalapino, and N. E. Bickers, “Knight shifts and nuclear-spin-relaxation rates for 2D model of CuO₂,” *Phys. Rev. B* **41**, 1797 (1990).
 - [32] J. Jaklič and P. Prelovšek, “Finite-Temperature conductivity,” *Phys. Rev. B* **50**, 7129 (1994).
 - [33] J. Jaklič and P. Prelovšek, “Finite-temperature properties of doped antiferromagnets,” *Adv. Phys.* **49**, 1–92 (2000).
 - [34] P. Prelovšek and J. Bonča, “Ground state and finite temperature lanczos methods,” in *Strongly Correlated Systems - Numerical Methods*, edited by A. Avella and F. Mancini (Springer, Berlin, 2013).
 - [35] D. D. Betts, S. Masui, N. Vats, and G. E. Stewart, “Improved finite-lattice method for estimating the zero-temperature properties of two-dimensional lattice models,” *Can. J. Phys.* **74**, 54–64 (1996).
 - [36] P. R. C. Kent, M. Jarrell, T. A. Maier, and Th. Pruschke, “Efficient calculation of the antiferromagnetic phase diagram of the three-dimensional hubbard model,” *Phys. Rev. B* **72**, 060411 (2005).
 - [37] See Supplemental Material for more details.
 - [38] B. Schmidt and P. Thalmeier, “Thermodynamics of anisotropic triangular magnets with ferro- and antiferromagnetic exchange,” *New J. Phys.* **17**, 073025 (2015).
 - [39] J. Kokalj and Ross H. McKenzie, “Thermodynamics of a bad metal–mott insulator transition in the presence of frustration,” *Phys. Rev. Lett.* **110**, 206402 (2013).
 - [40] Hazime Mori, “A continued-fraction representation of the time-correlation functions,” *Prog. Theor. Phys.* **34**, 399–416 (1965).
 - [41] D. Forster, *Hydrodynamic Fluctuations, Broken Symmetry, and Correlation Functions* (Bejamin/Cummings, Reading, MA, 1975) pp. 95-120.
 - [42] P. Prelovšek, I. Sega, and J. Bonča, “Scaling of the Magnetic Response in Doped Antiferromagnets,” *Phys. Rev. Lett.* **92**, 1–4 (2004).
 - [43] T. Moriya, “Nuclear magnetic relaxation in antiferromagnets,” *Prog. Theor. Phys.* **16**, 23–44 (1956).
 - [44] S. Chakravarty, B. I. Halperin, and D. R. Nelson, “2D quantum Heisenberg AFM at T > 0,” *Phys. Rev. B* **39**, 2344 (1989).

Supplemental Material for: Finite-temperature properties of the extended Heisenberg model on a triangular lattice

P. Prelovšek^{1,2} and J. Kokalj^{3,1}

¹*Jožef Stefan Institute, SI-1000 Ljubljana, Slovenia*

²*Faculty of Mathematics and Physics, University of Ljubljana, SI-1000 Ljubljana, Slovenia*

³*Faculty of Civil and Geodetic Engineering, University of Ljubljana, SI-1000 Ljubljana, Slovenia*

In the Supplemental Material we provide more details concerning the numerical method and tests, as well some additional results on thermodynamical quantities, the basic facts on the memory-function analysis and the presentation of dynamical quantities.

I. NUMERICAL METHOD AND THERMODYNAMICAL QUANTITIES

In the evaluation of thermodynamical (and further on dynamical) quantities we employ the FTLM method [1–3] on various triangular (and for comparison also square) lattices with periodic boundary conditions. The lattices with $N = 20 - 30$ sites are chosen so that they have a small imperfection [4, 5], but as well that they contain (if possible) characteristic points in the Brillouin zone. In particular this is the case for $\mathbf{Q}_K = (4\pi/3, 0)$ (the ordering wavevector of the spiral 120° order in triangular lattice) and $\mathbf{Q}_M = (0, 2\pi/\sqrt{3})$, ordering for the stripe-like order for $J_2 > 0.15$ and for the related standard AFM order on square lattice obtained as an extreme limit of anisotropic triangular lattice. Among the presented results, the largest lattice with $N = 30$ contains both points (see inset in Fig. 2 in the main text), while smaller lattices contain only some of them, e.g., $N = 26$ contains \mathbf{Q}_M but not \mathbf{Q}_K . Similar is the choice in presented results for the HM on the square lattice with $N = 30$ sites which contains the AFM ordering wavevector $\mathbf{Q}_M = (\pi, \pi)$.

The limitation of the present method is given by the size of the many-body Hilbert space with $N_{st} < 10^7$ basis states which can be handled efficiently within the FTLM, restricting the lattice sizes to $N \leq 30$. The main criterion for the macroscopic relevance of FTLM results is the thermodynamical sum $Z(T) = \text{Tr} \exp[-(H - E_0)/T]$, which determines the $Z > Z^* = Z(T_{fs}) \gg 1$. In addition, the FTLM approach also involves a random sampling over initial wavefunctions, which we typically choose $N_s = 10$, which partly influences the statistical error [2, 3] of results. We use the actual criterion that $Z^* \sim 10$ which implies (for $N = 30$) also roughly the threshold at entropy density $s(T_{fs}) \sim 0.1$, independent of the model. It is then evident that from Fig. 1 in the main text that T_{fs} depends essentially on the model. In particular, it follows that $T_{fs} \sim 0.4J$ for the square lattice HM, while $T_{fs} \sim 0.2J$ for the triangular lattice and $T_{fs} \sim 0.15J$ for frustrated lattice with $J_2 = 0.1$. While results at higher $T > T_{fs}$ do depend on the choice of the lattice, the actual behavior of various quantities, in particular of \mathbf{q} -dependent or \mathbf{q} -integrated dynamical quantities as

$1/T_1$, is more sensitive on the presence of relevant symmetry point in the Brillouin zone. On the other hand, thermodynamic quantities as $s(T)$, $C_V(T)$ and $\chi_0(T)$ are more robust, so results remain quite lattice-independent even at lower $T < T_{fs}$.

In Fig. 1 we present the results for the specific heat $C_V(T)$ on a triangular lattice with n.n. exchange only, i.e. with $J_2 = 0$, as obtained on different lattices with $N = 20 - 30$. It is evident that qualitative features of $C_V(T)$ are quite consistent and size independent down to $T \sim 0.15J$. All results share two essential features: a broad shoulder appearing below $T \sim J$ and a narrow coherence peak at $T \sim 0.2J$. Here, one should acknowledge that among presented thermodynamic quantities, C_V is the most sensitive on finite size effects. Hence, final results for $C_V(T)$ as well as for the entropy $s(T)$ for other model parameters as presented in Fig. 1 in the main text can be regarded as macroscopic ones down to $T \sim T_{fs}$.

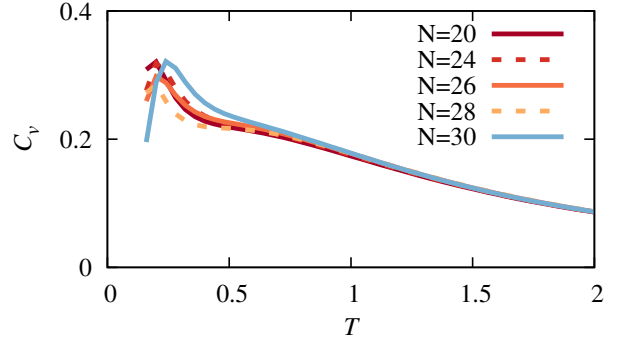


FIG. 1. Results for the specific heat $C_V(T)$ of the Heisenberg model on triangular lattice with $J_2 = 0$, as obtained by FTLM on systems with different number of sites $N = 20 - 30$.

In Fig. 2 we present also results for the uniform susceptibility $\chi_0(T)$. For the triangular lattice $\chi_0(T)$ are only weakly dependent on J_2 , at least for the accessible range $T > 0.15J$, since they all reveal maximum at $T^* \sim 0.4J$, in agreement (both in location and the value) with the high- T expansion result [6]. For comparison we show also the result for the square lattice with the maximum at $T^* \sim J$. While in the latter case the low- T limit is understood (due to long-range order at $T = 0$ one has

$\chi_0^0 = \chi_0(T \rightarrow 0) > 0$) [7], this is not the case for the frustrated triangular lattice with finite J_2 . In the case of $J_2 = 0$ (pure triangular lattice) one would expect in analogy with the square lattice $\chi_0^0 > 0$, while in the SL case, e.g., at $J_2 = 0.1$, the spin excitations can be either gapped with $\chi_0^0 = 0$ or gapless with $\chi_0^0 > 0$. Still, the restriction to $T > T_{fs}$ does not allow to differentiate between possible limits (finite or zero) of $\chi_0(T \rightarrow 0)$.

For completeness we show in Fig. 3 also the static spin structure factor $S_{\mathbf{q}}$ for chosen \mathbf{q} 's in the Brillouin zone.

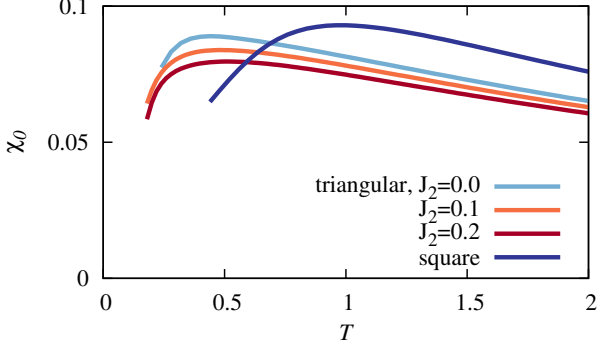


FIG. 2. Uniform spin susceptibility $\chi_0(T)$ within the Heisenberg model on the triangular lattice with $J_2 = 0 - 0.2$ and on the square lattice. Obtained by FTLM on $N = 30$ lattice.

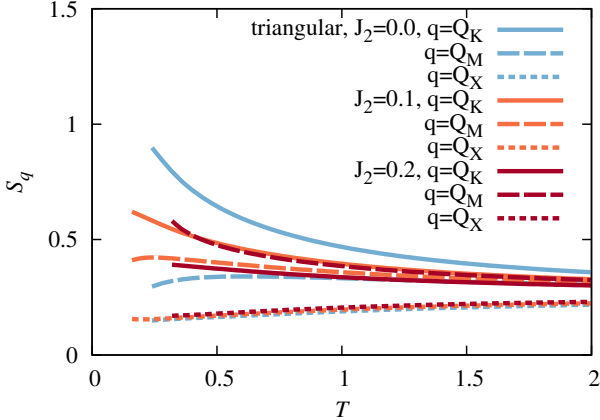


FIG. 3. Static spin structure factor $S_{\mathbf{q}}(T)$ for several wave-vectors \mathbf{q} calculated within the Heisenberg model on the triangular lattice with $J_2 = 0 - 0.2$. Obtained by FTLM on $N = 30$ lattice.

II. MEMORY-FUNCTION ANALYSIS

The dynamical spin susceptibility $\chi_{\mathbf{q}}(\omega)$ and the dynamical structure factor $S(\mathbf{q}, \omega)$ are defined in a standard

way,

$$\chi_{\mathbf{q}}(\omega) = i \int_0^\infty dt e^{i\omega t} \langle [S_{\mathbf{q}}^z(t), S_{-\mathbf{q}}^z(0)] \rangle,$$

$$\text{Im}\chi_{\mathbf{q}}(\omega) = \pi(1 - e^{-\beta\omega})S(\mathbf{q}, \omega), \quad (1)$$

The memory function (MF) formalism [8–10] is as usual introduced via the corresponding relaxation function $\Phi_{\mathbf{q}}(\omega)$,

$$\Phi_{\mathbf{q}}(\omega) = \frac{\chi_{\mathbf{q}}(\omega) - \chi_{\mathbf{q}}^0}{\omega}, \quad (2)$$

where $\chi_{\mathbf{q}}^0 = \chi_{\mathbf{q}}^0(\omega = 0)$ is static spin susceptibility. Then, one can generally represent the complex $\Phi_{\mathbf{q}}(\omega)$ in terms of the effective SW energy $\omega_{\mathbf{q}}$ and the (complex) SW damping function $M_{\mathbf{q}}(\omega)$,

$$\Phi_{\mathbf{q}}(\omega) = \frac{-\chi_{\mathbf{q}}^0}{\omega - \frac{\omega_{\mathbf{q}}^2}{\omega + M_{\mathbf{q}}(\omega)}}, \quad \omega_{\mathbf{q}}^2 = \frac{\eta_{\mathbf{q}}}{\chi_{\mathbf{q}}^0}, \quad (3)$$

leading with relation (2) to the Eq. (2) in the main text. In the formalism $\omega_{\mathbf{q}}$ is given as the (second) frequency moment of the relaxation function $\text{Im}\Phi_{\mathbf{q}}(\omega)$ with $\eta_{\mathbf{q}}$ being the corresponding 'stiffness',

$$\eta_{\mathbf{q}} = \frac{1}{\pi} \int_{-\infty}^{\infty} \omega \text{Im}\chi_{\mathbf{q}}(\omega) d\omega = \langle [[S_{\mathbf{q}}^z, H], S_{-\mathbf{q}}^z] \rangle \quad (4)$$

It is evident from the above relation to the static (rather local) quantity, that $\eta_{\mathbf{q}}$ is expected to be smoothly \mathbf{q} dependent as well weakly T dependent. From known $S(\mathbf{q}, \omega)$ we can now directly evaluate static quantities $\chi_{\mathbf{q}}^0$ and $\omega_{\mathbf{q}}$ and consequently from the complex $\chi_{\mathbf{q}}(\omega)$ (obtained via the Hilbert transform) we extract the MF function $M_{\mathbf{q}}(\omega)$,

$$M_{\mathbf{q}}(\omega) = \frac{\omega_{\mathbf{q}}^2}{\omega + \chi_{\mathbf{q}}^0/\Phi_{\mathbf{q}}(\omega)} - \omega, \quad (5)$$

in particular the SW damping function $\gamma_{\mathbf{q}}(\omega) = \text{Im}M_{\mathbf{q}}(\omega)$.

III. DYNAMICAL QUANTITIES

The analysis of $S(\mathbf{q}, \omega)$ in terms of the MF (3) is particularly meaningful, when the MF is considerably smoother, e.g., both in ω and in \mathbf{q} , than the corresponding original $S(\mathbf{q}, \omega)$ or $\Phi_{\mathbf{q}}(\omega)$.

In Fig. 4 we show imaginary part of the relaxation function $\text{Im}\Phi_{\mathbf{q}}(\omega)$, and its ω and \mathbf{q} dependence can be compared to the ω and \mathbf{q} of the memory function. In Fig. 5 we show imaginary part of MF $\gamma_{\mathbf{q}}(\omega)$, and demonstrate its weak ω and \mathbf{q} dependence for a range of T .

For completeness we show in Fig. 6 imaginary part of local relaxation function

$$\frac{\text{Im}\Phi_L(\omega)}{\pi} = \frac{1}{\pi N} \sum_{\mathbf{q}} \text{Im}\chi_{\mathbf{q}}(\omega)/\omega, \quad (6)$$

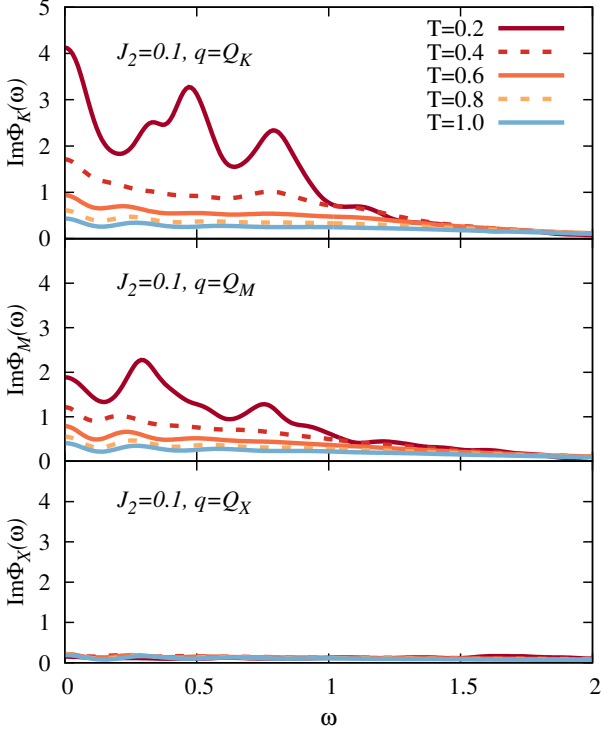


FIG. 4. Frequency dependence of the imaginary part of the relaxation function $\text{Im}\Phi_{\mathbf{q}}(\omega)$ for three characteristic $\mathbf{q} = \mathbf{Q}_K$, \mathbf{Q}_M and \mathbf{Q}_X . Calculated with FTLM on $N = 30$ lattice for $J_2 = 0.1$ and broadened with $\eta = 0.05$.

which is directly related to the NMR relaxation rate $1/T_1 = T\text{Im}\Phi_L(\omega)/\pi$ and shows smooth ω dependence and a decrease with T .

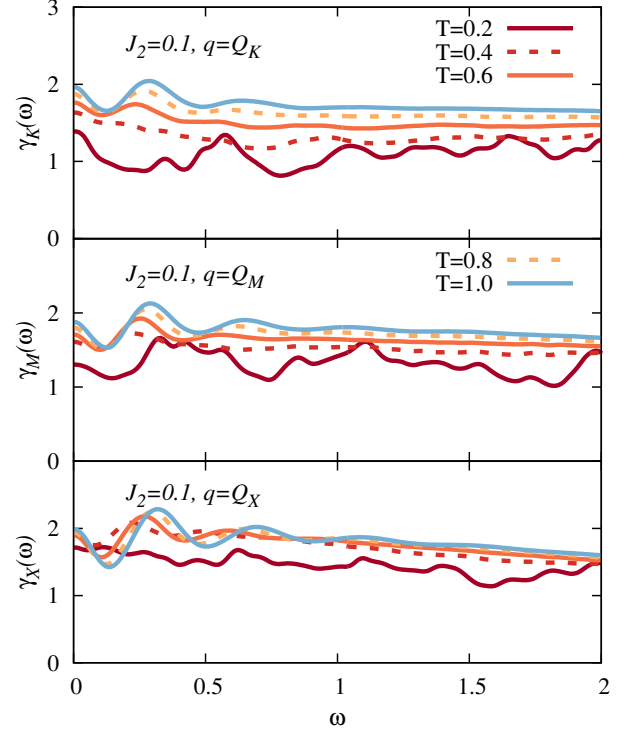


FIG. 5. Frequency dependence of the imaginary part of memory function, $\gamma_{\mathbf{q}}(\omega) = \text{Im}M_{\mathbf{q}}(\omega)$, for three characteristic $\mathbf{q} = \mathbf{Q}_K$, \mathbf{Q}_M and \mathbf{Q}_X . It is evident that $\gamma_{\mathbf{q}}(\omega)$ shows surprisingly small dependence on ω and \mathbf{q} , while it shows a decrease with T at lowest T as expected. Its value at $\omega = 0$ determines the NMR relaxation rate $1/T_1$. Calculated with FTLM on $N = 30$ lattice for $J_2 = 0.1$ and broadened with $\eta = 0.05$.

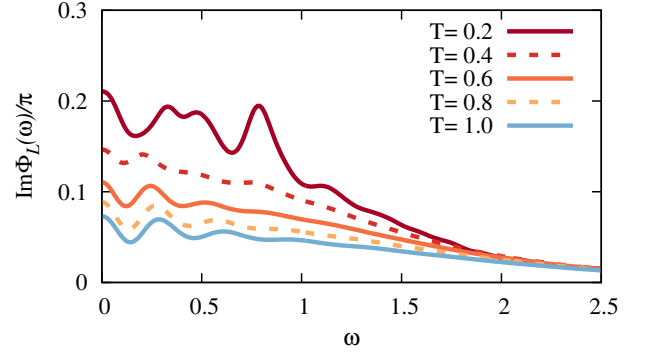


FIG. 6. Frequency dependence of the local $\text{Im}\Phi_L(\omega)/\pi$ for several T . Calculated with FTLM on $N = 30$ lattice for $J_2 = 0.1$ and broadened with $\eta = 0.05$.

-
- [1] J. Jaklič and P. Prelovšek, [Phys. Rev. B **50**, 7129 \(1994\)](#).
 - [2] J. Jaklič and P. Prelovšek, *Adv. Phys.* **49**, 1 (2000).
 - [3] P. Prelovšek and J. Bonča, in *Strongly Correlated Systems - Numerical Methods*, edited by A. Avella and F. Mancini (Springer, Berlin, 2013).
 - [4] D. D. Betts, S. Masui, N. Vats, and G. E. Stewart, *Can. J. Phys.* **74**, 54 (1996).
 - [5] P. R. C. Kent, M. Jarrell, T. A. Maier, and T. Pruschke, [Phys. Rev. B **72**, 060411 \(2005\)](#).
 - [6] N. Elstner, R. Singh, and a. Young, [Phys. Rev. Lett. **71**, 1629 \(1993\)](#).
 - [7] E. Manousakis, *Rev. Mod. Phys.* **63** (1991).
 - [8] H. Mori, [Prog. Theor. Phys. **34**, 399 \(1965\)](#).
 - [9] D. Forster, *Hydrodynamic Fluctuations, Broken Symmetry, and Correlation Functions* (Bejamin/Cummings, Reading, MA, 1975) pp. 95-120.
 - [10] P. Prelovšek, I. Sega, and J. Bonča, [Phys. Rev. Lett. **92**, 1 \(2004\)](#).